Performance and Stability of Plasma-Sprayed 10 × 10 cm² Self-sealing Metal-Supported Solid Oxide Fuel Cells

Jiu-Tao Gao[1] · Jia-Hong Li[1] · Yue-Peng Wang[1] · Chang-Jiu Li[1] · Cheng-Xin Li[1]

Abstract This study adopts a novel structure design of large-area planar metal-supported solid oxide fuel cell (MS-SOFC), which exhibits the characteristics of self-sealing and high thermal cycling resistance. The self-sealing structure of MS-SOFCs is achieved by brazing technology. Plasma spraying is performed to prepare all functional layers of cells. The size of cells is 10 × 10 cm². The coefficients of thermal expansion of relevant parts (i.e., porous metal support, interconnector and compound structure of both) and the electrical conductivity of brazing solder were measured. The microstructure of brazing area was observed in situ at 800 °C for 500 h, and the distribution of fuel gas in the interconnector was simulated. The performance of cells was characterized and found that the maximum power density can reach up to 716 mW cm^{-2} at 700 °C. Moreover, the long-term stability of the cell was investigated for about 500 h with 6 times of thermal cycling implemented during this period. The open circuit voltage and the maximum power density of the cell showed a good stability.

Keywords Long term · Metal-supported solid oxide fuel cells · Plasma spraying · Self-sealing · Thermal cycling

Introduction

Solid oxide fuel cells (SOFCs) can directly convert chemical energy into electrical energy through electrochemical reactions, which is very efficient (Ref 1-3). As the third generation of SOFCs, in the recent years, metal-supported SOFCs (MS-SOFCs) have received more attention (Ref 4-6). Compared with traditional ceramic SOFC, they have many advantages, such as low cost, high thermal conductivity, high mechanical strength, high electrical conductivity, improved heat resistance and fast start-up performance (Ref 7-9). Although MS-SOFC has many advantages, due to the different physical or chemical properties of metal and ceramic components, the traditional manufacturing processes still have many limitations (Ref 10, 11). Most of ceramic materials for SOFCs need to be sintered at a very high temperature oxidizing atmosphere (> 1200 °C). However, due to severe oxidation, metal supports are not allowed to be heated in an oxidizing atmosphere at a high temperature.

In order to solve this problem, many efforts have been made in recent years (Ref 12-14). As a fast and economical method of manufacturing coatings, plasma spraying has unique advantages. Not only because this technology is not limited by the shape and size of objects, but also because it can reduce the thermal effect on the substrate due to the rapid deposition process. Many problems [e.g. the oxidation of substrate (Ref 11), interaction between layers (Ref 15)] can be avoided, which are usually caused by conventional high-temperature co-sintered process. In addition, changes in composition or coating microstructure can be easily achieved by adjusting spraying parameters (Ref 16), which is essential for improving cell performance. Many extended works on plasma spraying of electrodes have been done (Ref 17-19). In order for the gas to enter

✉ Cheng-Xin Li
licx@mail.xjtu.edu.cn

1   State Key Laboratory for Mechanical Behavior of Materials, School of Materials Science and Engineering, Xi'an Jiaotong University, Xi'an, Shaanxi, China

the interface area between the electrode and the electrolyte, it must exhibit high porosity. It has been reported that a gradient microstructure of coatings can be built up in a continuous process by varying the spraying parameters (Ref 20). As the core component of SOFCs, electrolytes need the highest quality requirement. Due to the low electrical conductivity, the thickness of electrolyte layers should be thin (usually < 80 μm) to avoid excessive internal resistance, at the same time, its structure must be dense to prevent fuel gas and oxygen from meeting. Moreover, the degradation of electrodes will be increased due to the gas leakage. Literature reveals that, due to the optimized combination of layers, it is possible to deposit electrolyte layers with higher electrical conductivity and gas-tightness through plasma spraying by increasing the deposition temperature and particle speed. Coating with different microstructures can be prepared by plasma spraying which are significantly important to meet the different requirements of functional layers of SOFCs (e.g., porous anode and cathode, and dense electrolyte).

Moreover, for conventional planar SOFCs, how to seal cells is a big issue (Ref 21-23). The CET of cathode materials (like $La_{0.6}Sr_{0.4}Co_{0.2}Fe_{0.8}O_3$) is about 15.3×10^{-6} K^{-1} (Ref 24). The CET of typical electrolyte materials (like Y_2O_3-stabilized ZrO_2 (YSZ)) is reported about 10.1×10^{-6} K^{-1} (Ref 25). Metallic materials, including supports and interconnectors, such as SUS430, Crofer 22 and ZMG232L, have CTE of 12×10^{-6} K^{-1} (Ref 26), 10×10^{-6} K^{-1} (Ref 26) and 11×10^{-6} K^{-1} (Ref 27), respectively. When a glass sealant is used to seal the cell plate with interconnector, it is easy to lead to stress generation due to the difference in the CTE between different components. This problem seriously affects the reliability of glass sealing which in turn limits the MS-SOFC's quick start up ability. Therefore, the sealing problem of planar MS-SOFCs should be solved.

In this study, a novel structure of MS-SOFCs is designed to achieve the self-sealing characteristics of MS-SOFCs. Welding technology is adopted to the anode side, because of the weldability of metal support and interconnector. The functional layers of MS-SOFCs are prepared through plasma spraying additive manufacturing. The performance of MS-SOFCs and the long-term stability of the cell under thermal cycling were investigated.

Experiments

Self-sealing Structure of MS-SOFCs

The schematic for self-sealing MS-SOFCs is shown in Fig. 1(a). The thickness of the porous metal support (SUS 430) is about 1 mm, and it is bonded well with an interconnector (SUS 430) through brazing technology. Some Ni-based solder is pasted to the edges of the interconnector. After that porous metal support and the interconnector are assembled together and sintered in a vacuum furnace. Figure 1(b) demonstrates the parameter of brazing process. The melting point of solder (1000 °C) is significantly higher than the MS-SOFCs operating temperature (700 °C). In this experiment, flux-free furnace brazing was performed under a high vacuum of 10^{-2} Pa. The surfaces of different parts for joining were carefully cleaned with acetone.

Fabrication of Functional Layers

Table 1 shows the parameters for the preparation of MS-SOFC functional layers. Atmospheric plasma spraying (APS) (GDP-80, Jiujiang, 80 kW class) was used to deposit a thin anode layer of 15-25 μm on the porous metal support with composite powder (50/50 wt.%) of NiO and GDC (10 mol.%-Gd_2O_3-doped CeO_2) (TERIO CORPORATION, N80898) (20-50 μm). The plasma torch was operated at 35 kW. Spraying distance during deposition was kept 100 mm. The electrolyte layer about 40-55 μm was prepared by using very low-pressure plasma spraying (VLPPS) (MF-P 1000 APS/VPS, GTV, Germany) at 250 mm with ScSZ (10 mol.%-Sc_2O_3-stabilized ZrO_2) (FUJIMI, 565E5) fused crushed powders (5-25 μm). $La_{0.6}Sr_{0.4}Co_{0.2}Fe_{0.8}O_3$ (LSCF) (METCO, 6830A) powder with the particle size distribution of 20-70 μm was employed for cathode deposition. The morphology of powders is shown in Fig. 2. The LSCF cathode layer of 9×9 cm^2 area was deposited by APS with a plasma arc power of 30 kW and 20-30 μm thickness. The spraying distance was 100 mm.

Characterization of MS-SOFCs

The brazing material was prepared into wafers (the diameter is 10 mm and the thickness is 1 mm). The electrical conductivity of brazing solder itself was measured using 4-wire at 800 °C for 500 h (Solartron SI 1260/1287). The CTE of porous metal support, interconnector material and compound structure of both were also measured in the temperature range from 200 to 800 °C (NETZSCH DIL 402C). The test samples for CTE were cylindrical, with a diameter of 4 mm and a length of 20 mm. The bond line run the length of the cylinder and it was situated at the midline so that equal volumes of support and interconnector were in the specimen. The microstructure of brazing area was observed in situ at 800 °C in air for 500 h by scanning electron microscopy (SEM, VEGA II-XMU, TESCAN, Czech). It was a single sampled observed at different time

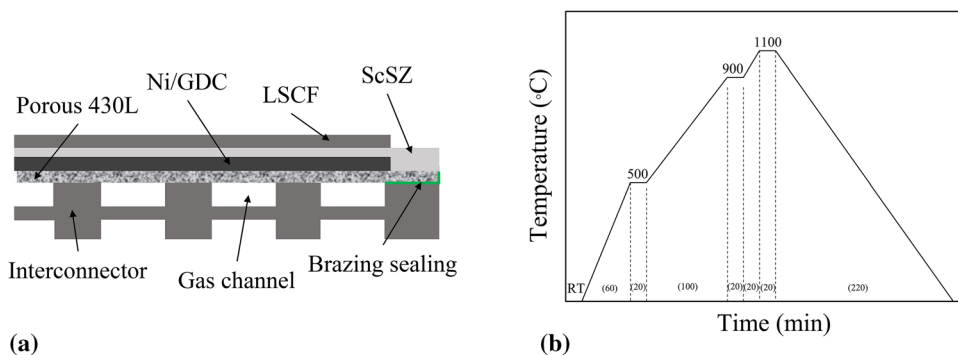Fig. 1 (a) Schematic representation of self-sealing MS-SOFCs; (b) parameters of brazing process

Table 1 Plasma spraying parameters for preparing functional layers of MS-SOFCs

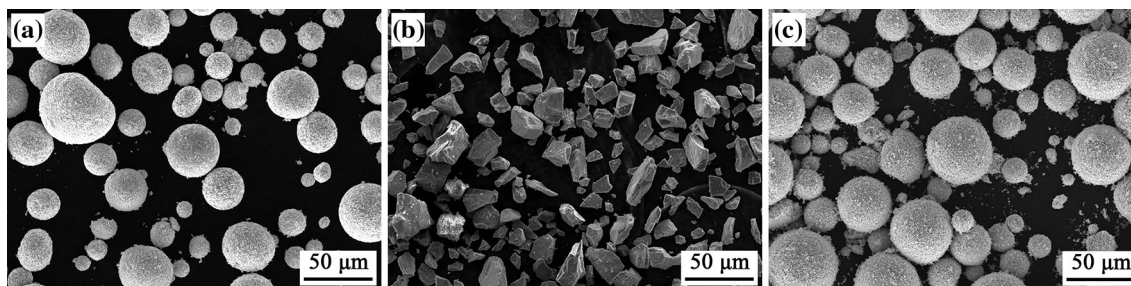| Parameters	Anode	Electrolyte	Cathode
Methods	APS	VLPPS	APS
Powders	NiO/GDC	ScSZ	LSCF
Power, kW	35	60	30
Current, A	500	680	500
Gas components, L min^{-1}	Ar/H$_2$ (50/3)	Ar/H$_2$ (60/10)	Ar/H$_2$ (50/1)
Spraying distance, mm	100	250	100
Torch traverse speed, mm s^{-1}	450	550	450
Powder feed rate, g min^{-1}	4.5	6	5

Fig. 2 Morphology of the powders: (a) Ni/GDC; (b) ScSZ; (c) LSCF

intervals. The surface of the sample was polished before each observation.

In order to check the suitability of the structure of the interconnector, the fuel gas distribution in the interconnector was simulated by the finite element commercial software COMSOL MULTIPHYISCS Version 5.4. The physical field control mesh was set up and triangle size was in the range of 0.04-38.8 μm with 119,217 degrees of freedom. The inlet gas flow rate was set to 0.5 slm and the outlet pressure was set to 1 atm.

The size of the MS-SOFC is 10×10 cm^2. Another interconnector was used for current conduction and air supply at cathode side, as shown in Fig. 3. A thin layer of LSCF paste was used as a current collector at cathode side, and because of the metal support, an additional current collector was not required on the anode side. The output performance of the cell was tested using a SourceMeter (2440 5A SourceMeter, KEITHLEY, USA) with wet
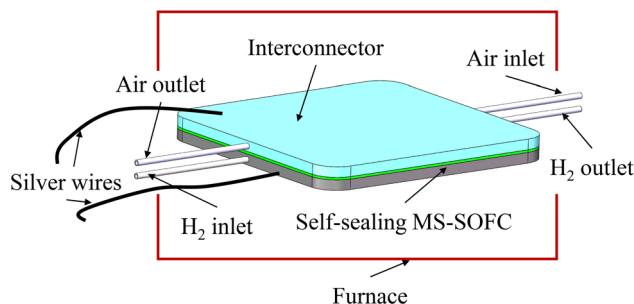

Fig. 3 Schematic representation of the self-sealing MS-SOFC testing

hydrogen fuel (3% H$_2$O 0.5 slm) and air (2 slm). 6 thermal cycles were implemented during 500 h. Each thermal cycling was from 550 to 700 °C then to 550 °C, and the heating and cooling rates were 5 °C min^{-1}. Before next thermal cycling, the MS-SOFC was kept at 550 °C under open circuit condition.

Results and Discussion

Welded Interconnect and Support

The CTE of porous metal support, interconnector material and compound structure of both were measured in the temperature range of 200-800 °C. Fig. 4 shows the relative length change of these samples as a function of temperature in air at a heating rate of 5 °C min^{-1}. The CTEs of these parts slowly increase with an increase in temperature. The values are in the range of 11×10^{-6} K^{-1}-12×10^{-6} K^{-1}. The CTE of the welded component is slightly lower than the CTE of porous metal support. It is beneficial for the cell, because the value is closer to ScSZ electrolyte [10.1×10^{-6} K^{-1} (Ref 28)].

The electrical conductivity of most metal materials decreases with increasing of temperature (Ref 29). Figure 5 shows the change in electrical conductivity of the brazing solder with time. The initial electrical conductivity of the brazing solder reached to almost 800 S cm^{-1}. Whereas it was slightly decreased in the first 200 h, after that, the high electrical conductivity is gradually stabilizing and the value is above 700 S cm^{-1} for the last 300 h without any observable degradation that was demonstrating its high stability. Typically, it is considered that the ohmic resistance of SOFCs is attributed to the electrolyte layer. The electrical conductivity of the brazing solder is above 700 S cm^{-1} at 800 °C during this period. A typical range of electrical conductivity expected for an anode operating at 1000 °C is 100-400 S cm^{-1} (Ref 30), and the electrical conductivity of ScSZ electrolyte at 800 °C is ~ 0.1 S cm^{-1} (Ref 31) which is almost four orders lower than the brazing solder electrical conductivity. It indicates
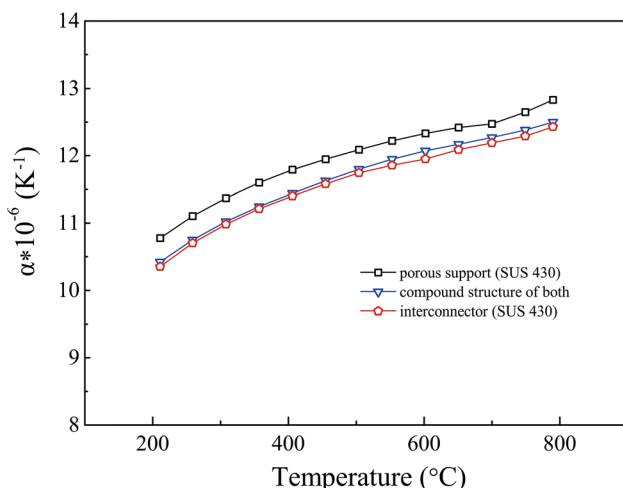
that the ohmic losses caused by the brazing process are negligible.

Figure 6 illustrates in situ observed results of the cross-sectional microstructure of the brazing sealing between porous metal support and interconnector after 800 °C heat treatment during different time intervals. Figure 6(a) and (b) shows the original morphology of the interface between porous metal support and interconnector. Furnace brazing is used to join metal support and interconnector with Ni-based solder, which reveals good wetting of the materials when brazed at 1100 °C for 10 min. Owing to good wetting of Ni-based solder, remarkable adhesion between metal support and interconnector can be observed. It shows a well-bonded interface between the porous metal support and interconnector. For MS-SOFC new structure, sufficient gas tightness is important to obtain a high open circuit voltage and to guarantee the safety of the system. Figure 6(c) and (d) shows the morphology of the area after 100 h heat treatment at 800 °C. No remarkable changes can be observed in the interface area but some oxides are growing in the porous metal support. Figure 6(e) and (f) shows the morphology of the area after 200 h treatment at 800 °C. Compared with Fig. 6(c) and (d), there is nothing happened except more oxide in the porous support. Figure 6(g) and (h) shows the morphology after 500 h at 800 °C. The interface area is still stable. These results illustrate that the brazing sealing structure is sufficiently stable for the safe operation of MS-SOFCs.

Distribution of Fuel Gas

Figure 7(a) shows the schematic representation of inter-connector. The depth of the fuel gas channel is 0.5 mm. The size of raised little squares is 3×3 mm^2 and the interval between them is 5 mm. Inlet and outlet of fuel gas

Fig. 4 CTE of interconnect, support and compound structure of both at the range of temperature between 200 and 800 °C
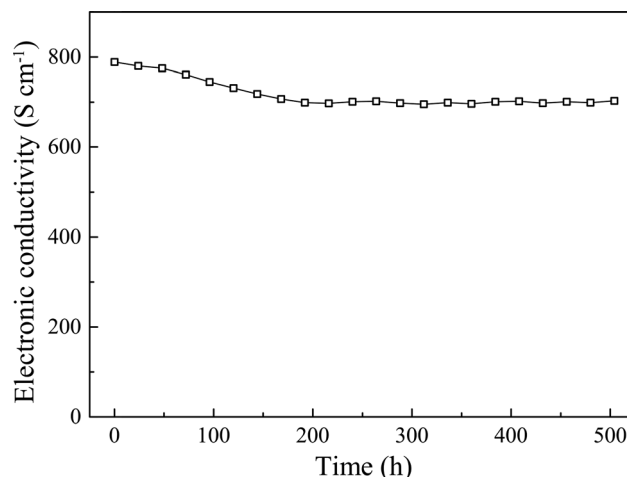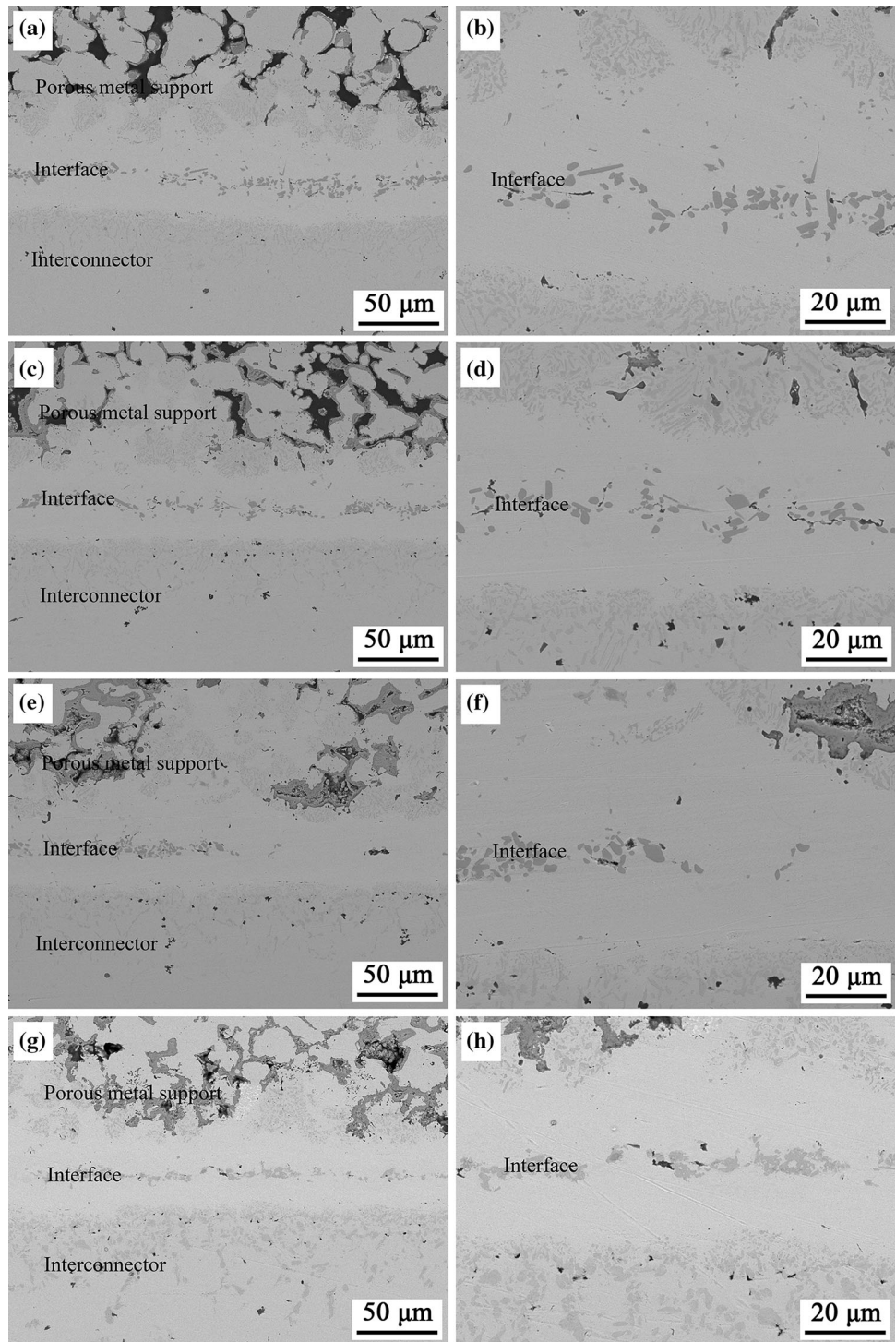

Fig. 5 Electrical conductivity of the brazing solder in air at 800 °C for 500 h

Fig. 6 In situ observing for brazing sealing stability at 800 °C at different time: (a, b) 0 h; (c, d) 100 h; (e, f) 200 h; (g, h) 500 h

are located at symmetrical sides with diameter of 1.5 mm. Figure 7(b) and (c) shows the simulation results at the middle position (i.e. 0.25 mm) of gas channel. Figure 7(b) is the distribution of fuel gas pressure in the interconnector. The highest pressure for the fuel gas is at the inlet position and the lowest is at the outlet position. Although pressure gradient exists in the interconnector channel, the pressure difference is almost negligible. In other words, fuel gas pressure in the interconnector is uniform. The velocity distribution of fuel gas in the interconnector is shown in Fig. 7(c). The highest flow velocity occurs at the inlet and outlet. The average velocity of the fuel gas is about 0.1 m s^{-1}. Due to uniform distribution of fuel gas in the interconnector, the structure design is logical
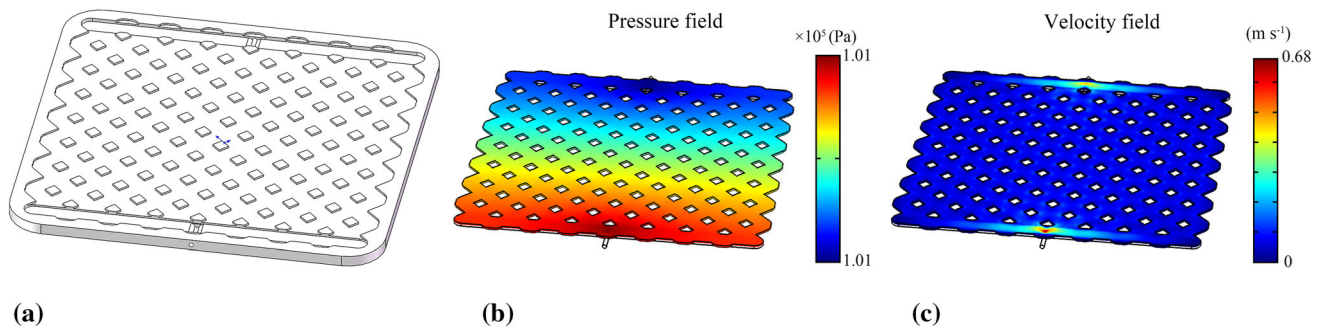
Fig. 7 Distribution of fuel gas at anode side in the interconnector: (a) schematic representation of interconnector; (b) pressure distribution; (c) velocity distribution
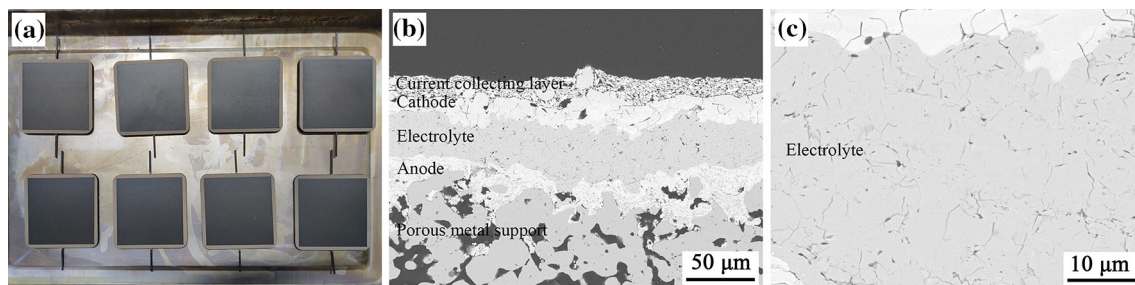

Fig. 8 Morphology of MS-SOFCs: (a) finished products; (b) microstructure of cross section; (c) magnified morphology of the electrolyte layer

and effective. To summarize, fuel gas is evenly distributed in the cell at the anode side by applying this structure, which is beneficial to improve the performance of the MS-SOFC (Ref 32, 33).

Microstructure

The finished products of MS-SOFCs are shown in Fig. 8(a). The area of these cells is 10×10 cm^2 with an effective electrode of 9×9 cm^2. Each cell has two thin pipes as the inlet/outlet of fuel gas. Self-sealing property is achieved at anode side. Figure 8(b) shows the cross-sectional microstructure of the plasma-sprayed MS-SOFCs. The thicknesses of the anode layer, the electrolyte layer and the cathode layer are 15-25, 40-55 and 20-30 μm, respectively. A good bonding is formed between the adjacent layers, which is advantageous for the minimization of the contact resistance inside the functional layers. The large sinuosity of electrolyte surface contributes to increase length of triple phase boundary and improve the electrochemical performance of cells (Ref 34, 35). Cracks and voids can be seen in anode and cathode layers, which ensure the diffusion of fuel gas and oxygen. VLPPS technology is employed to prepare electrolyte layers. Because of lower surrounding pressure, the plasma flow is greatly expanded (Ref 36, 37). It helps to increase the speed and temperature of particles. According to literature, the interior bonding of ceramic

coatings can be improved by increasing the speed and temperature of particles (Ref 38, 39). The upgrading of lamellar bonding in the electrolyte coatings is not only responsible to enhance the gas tightness, but it also contributes to improve its electrical conductivity (Ref 40).

Output Performance

The output performance curves of the cell at 550, 600, 650 and 700 °C are shown in Fig. 9. The OCVs obtained for the MS-SOFC at 550, 600, 650 and 700 °C are 1.028, 1.026, 1.025 and 1.019 V, respectively. In addition, the maximum power density of the cell is 196, 284, 438 and 716 mW cm^{-2} at 550, 600, 650 and 700 °C, respectively. The output performance of different cells prepared by several methods is shown in Table 2. Despite the large effective area (9×9 cm^2) of the cell used in this experiment, it still exhibits a good output performance.

As mentioned above, conventional plasma spraying processing produces a lamellar and porous microstructure, which leads to low OCV and cell efficiency. The OCV of SOFCs with electrolyte layers directly prepared by APS is typically about 0.9 V (Ref 41). It has been reported that the thickness of 250 μm is required to guarantee the gas tightness of electrolyte layers deposited by APS (Ref 42). However, due to the low electrical conductivity, the considerable thickness of electrolyte layer can cause serious

ohmic polarization losses. The results of this experiment demonstrate that the use of the VLPPS technique to prepare the electrolyte layer is a good choice. Although some micro-cracks and voids are still present in the electrolyte layer, the interface bonding between lamellas is improved; thus, the electrical conductivity of electrolyte layer is increased. In the rapid solidification process, it is inevitable to create cracks in ceramic coatings prepared by plasma spraying. During the splat cooling, a large temperature gradient is formed between the solidified splat and the substrate. The quenching stress causes cracks in splats (Ref 43). On the other hand, the improved interface bonding forces the quenching stress developed along the vertical direction. Therefore, some micro-vertical cracks can still be observed in the electrolyte layer.

The cell shows good output performance not only due to the electrolyte layer, but also include other factors (i.e., plasma-sprayed anode and cathode, metal support). Generally, porosity of coatings prepared by plasma spraying is ranging from 5 to 15 vol.% (Ref 44, 45). However, in order to improve the gas diffusion, the expected porosity level for the SOFC anodes is ∼ 40 vol.% (Ref 46, 47), which is much higher than the porosity directly obtained by plasma spraying. In the process of reducing the NiO composition to Ni, the porosity of anode coatings will further increase and the growth of porosity depends on the percentage of NiO in the original anode powder. A low porosity of the

anode may severely deteriorate the performance of anode supported cells. Fortunately, because the anode layer is directly deposited on porous metal supports in this work, its thickness is as low as 15-25 μm, so the low porosity will not have a substantial impact on the electrochemical performance of the cell. Many cracks are formed in cathode layer, which is conductive to oxygen diffusion. At the same time, due to the large interface between functional layers, the length of three phase boundary is increased, which is of great significance for improving the electrochemical performance of the cell. Therefore, layers met different requirements for SOFCs can be prepared by plasma spraying only through adjusting the spraying parameters.

Long-Term Stability

Figure 10(a) shows the operating parameters of long-term testing. Generally, two major factors should be considered as the cause of SOFC thermal cycle degradation (Ref 52-54). Because of the dramatical change of thermal stress, cracks can be easily created in ceramic components of SOFCs, especially in electrolyte layer (Ref 55-57). Gas leakage will happen at the internal SOFCs. The gas partial pressure at both anode side and cathode side will change; then the OCV of the cell will decrease. Moreover, it is harmful to the performance of electrode materials. Another factor is the modified electrode structure. The bonding between conductive phase of electrode is reduced due to the sintering effect (usually occurs at the anode). The electrical conductivity and the effective area of electrode are both reduced. Usually, this does not affect the OCV of SOFCs, but is closely related to their output performance. So, the OCV and the power density are both needed to measure and evaluate the effect of thermal cycling on the performance stability of MS-SOFCs. Figure 10(b) shows the values of the OCV and the maximum power density of the cell at 650 °C during long-term testing period. Very little change in OCV is observed during this process. The maximum power density has some slight downs during this period. Maybe this is because of the oxidation and reduction effect occurs in the anode (Ref 58, 59). This hypothesis can partly explain this fluctuation trend. It suggests that the degradation of the MS-SOFC may be caused by the changes in microstructure of electrodes. Further research
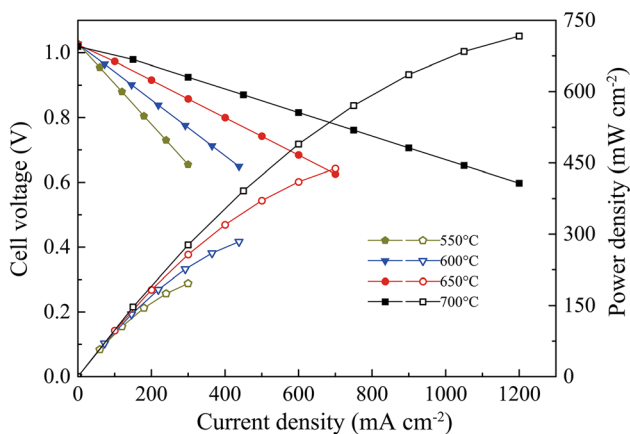
Fig. 9 Output performance of the cell

Table 2 Maximum power density of several cells prepared by different methods

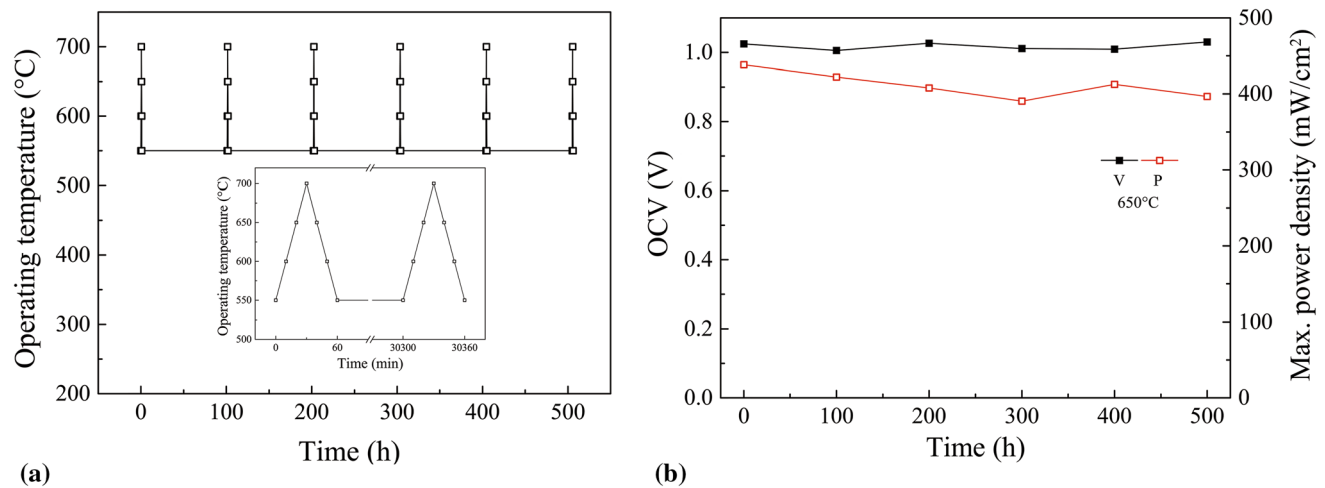| Cell materials	T, °C	Maximum power density, mW cm^{-2}	Method	References
NiO/GDC‖ScSZ‖LSCF	700	716	Plasma spraying	This work
NiO/YSZ‖LSGM‖LSCF	800	710	Plasma spraying	Ref 48
NiO/YSZ‖YSZ‖LSM	800	810	Sintering	Ref 49
NiO/YSZ‖YSZ‖LSM	850	530	Sintering	Ref 50
NiO/YSZ‖YSZ‖Au	800	800	EB-PVD	Ref 51

Fig. 10 (a) Operating temperature curve during thermal cycling process; (b) the stability of OCV and Max. power density of the cell at 650 °C

will be conducted to find out more details and explain this phenomenon more reasonably.

Conclusion

Self-sealing MS-SOFCs were designed and prepared by plasma spraying. The electrical conductivity of the brazing solder is measured at 800 °C for 500 h which maintains above 700 S cm^{-1}, indicating its high stability. In situ observed results show that the long-term stability of the brazing sealing is reliable. The simulation results of the gas distribution show that the structure of the interconnector is capable to meet the requirements for MS-SOFC operation. OCVs of the MS-SOFC are all above 1.0 V in the operating temperature range, and the maximum power density is 196, 284, 438 and 716 mW cm^{-2} at 550, 600, 650 and 700 °C, respectively. The long-term performance of MS-SOFCs is tested for 500 h. During this period, 6 thermal cycles are implemented and the MS-SOFC is kept at 550 °C under open circuit condition at the rest of the time. The OCV and the maximum power density of the cell show a good stability.

References

1. F. Ramadhani, M.A. Hussain, H. Mokhlis and S. Hajimolana, Optimization Strategies for Solid Oxide Fuel Cell (SOFC) Application: A Literature Survey, *Renew. Sustain. Energy Rev.*, 2017, **76**, p 460–484.

2. M. Mehrpooya, M. Sadeghzadeh, A. Rahimi and M. Pouriman, Technical Performance Analysis of a Combined Cooling Heating and Power (CCHP) System Based on Solid Oxide Fuel Cell (SOFC) Technology: A Building Application, *Energy Convers. Manag.*, 2019, **198**, p 111767.

3. E. Shayan, V. Zare and I. Mirzaee, On the Use of Different Gasification Agents in a Biomass Fueled SOFC by Integrated Gasifier: A Comparative Exergo-Economic Evaluation and Optimization, *Energy*, 2019, **171**, p 1126–1138.

4. P. Blennow, J. Hjelm, T. Klemensø, S. Ramousse, A. Kromp, A. Leonide and A. Weber, Manufacturing and Characterization of Metal-Supported Solid Oxide Fuel Cells, *J. Power Sources*, 2011, **196**(17), p 7117–7125.

5. V.V. Krishnan, Recent Developments in Metal-Supported Solid Oxide Fuel Cells, *Wiley Interdiscip. Rev. Energy Environ.*, 2017, **6**(5), p e246.

6. F. Thaler, D. Udomsilp, W. Schafbauer, C. Bischof, Y. Fukuyama, Y. Miura, M. Kawabuchi, S. Taniguchi, S. Takemiya, A. Nenning, A.K. Opitz and M. Bram, Redox Stability of Metal-Supported Fuel Cells with Nickel/Gadolinium-Doped Ceria Anode, *J. Power Sources*, 2019, **434**, p 226751.

7. M.C. Tucker, G.Y. Lau, C.P. Jacobson, L.C. DeJonghe and S.J. Visco, Performance of Metal-Supported SOFCs with Infiltrated Electrodes, *J. Power Sources*, 2007, **171**(2), p 477–482.

8. M.C. Tucker, Progress in Metal-Supported Solid Oxide Fuel Cells: A Review, *J. Power Sources*, 2010, **195**(15), p 4570–4582.

9. P. Blennow, J. Hjelm, T. Klemensø, Å.H. Persson, S. Ramousse and M. Mogensen, Planar Metal-Supported SOFC with Novel Cermet Anode, *Fuel Cells*, 2011, **11**(5), p 661–668.

10. H. Kurokawa, K. Kawamura and T. Maruyama, Oxidation Behavior of Fe-16Cr Alloy Interconnect for SOFC Under Hydrogen Potential Gradient, *Solid State Ion.*, 2004, **168**(1), p 13–21.

11. I. Antepara, I. Villarreal, L.M. Rodríguez-Martínez, N. Lecanda, U. Castro and A. Laresgoiti, Evaluation of Ferritic Steels for Use as Interconnects and Porous Metal Supports in IT-SOFCs, *J. Power Sources*, 2005, **151**, p 103–107.

12. J. Oberste Berghaus, J.G. Legoux, C. Moreau, R. Hui, C. Decès-Petit, W. Qu, S. Yick, Z. Wang, R. Maric and D. Ghosh, Suspension HVOF Spraying of Reduced Temperature Solid Oxide Fuel Cell Electrolytes, *J. Therm. Spray Technol.*, 2008, **17**(5), p 700–707.

13. N.P. Brandon, A. Blake, D. Corcoran, D. Cumming, A. Duckett, K. El-Koury, D. Haigh, C. Kidd, R. Leah, G. Lewis, C. Matthews, N. Maynard, N. Oishi, T. McColm, R. Trezona, A. Selcuk, M. Schmidt and L. Verdugo, Development of Metal Supported Solid Oxide Fuel Cells for Operation at 500-600 °C, *J. Fuel Cell Sci. Technol.*, 2004, **1**(1), p 61–65.

14. M.C. Tucker, G.Y. Lau, C.P. Jacobson, L.C. DeJonghe and S.J. Visco, Stability and Robustness of Metal-Supported SOFCs, *J. Power Sources*, 2008, **175**(1), p 447–451.

15. W.G. Bessler, A new computational approach for SOFC impedance from detailed electrochemical reaction–diffusion models, *Solid State Ion.*, 2005, **176**(11), p 997–1011.

16. A.E. Giannakopoulos, S. Suresh, M. Finot and M. Olsson, Elastoplastic Analysis of Thermal Cycling: Layered Materials with Compositional Gradients, *Acta Metall. Mater.*, 1995, **43**(4), p 1335–1354.

17. Y. Ohno, Y. Kaga and S. Nagata, A Study on the Fabrication and the Performance of the Solid Electrolyte Fuel Cell, *Electr. Eng. Jpn.*, 1987, **107**(1), p 59–67.

18. Y. Liu, S. Zha and M. Liu, Nanocomposite Electrodes Fabricated by a Particle-Solution Spraying Process for Low-Temperature SOFCs, *Chem. Mater.*, 2004, **16**(18), p 3502–3506.

19. P. Holtappels, C. Sorof, M.C. Verbraeken, S. Rambert and U. Vogt, Preparation of Porosity-Graded SOFC Anode Substrates, *Fuel Cells*, 2006, **6**(2), p 113–116.

20. R. Hui, Z. Wang, O. Kesler, L. Rose, J. Jankovic, S. Yick, R. Maric and D. Ghosh, Thermal Plasma Spraying for SOFCs: Applications, Potential Advantages, and Challenges, *J. Power Sources*, 2007, **170**(2), p 308–323.

21. R.N. Singh, Sealing Technology for Solid Oxide Fuel Cells (SOFC), *Int. J. Appl. Ceram. Technol.*, 2007, **4**(2), p 134–144.

22. F. Smeacetto, M. Salvo, M. Ferraris, J. Cho and A.R. Boccaccini, Glass–Ceramic Seal to Join Crofer 22 APU Alloy to YSZ Ceramic in Planar SOFCs, *J. Eur. Ceram. Soc.*, 2008, **28**(1), p 61–68.

23. J. Puig, A. Prange, B. Arati, C. Laime, P. Lenormand and F. Ansart, Optimization of the Synthesis Route of a Barium Boron Aluminosilicate Sealing Glass for SOFC Applications, *Ceram. Int.*, 2017, **43**(13), p 9753–9758.

24. L.W. Tai, M.M. Nasrallah, H.U. Anderson, D.M. Sparlin and S.R. Sehlin, Structure and Electrical Properties of $La_{1-x}Sr_xCo_{1-y}$-$FeyO_3$. Part 2. The system $La_{1-x}Sr_xCo_{0.2}Fe_{0.8}O_3$, *Solid State Ion.*, 1995, **76**(3–4), p 273–283.

25. M. Mukhopadhyay, J. Mukhopadhyay, A.D. Sharma and R.N. Basu, Ball Mill Assisted Synthesis of Ni–YSZ Cermet Anode by Electroless Technique and Their Characterization, *Mater. Sci. Eng. B*, 2009, **163**(2), p 120–127.

26. S. Fontana, R. Amendola, S. Chevalier, P. Piccardo, G. Caboche, M. Viviani, R. Molins and M. Sennour, Metallic Interconnects for SOFC: Characterisation of Corrosion Resistance and Conductivity Evaluation at Operating Temperature of Differently Coated Alloys, *J. Power Sources*, 2007, **171**(2), p 652–662.

27. T. Ohno, A. Toji, T. Uehara, G. Bao and S. Imano, Development of Low Thermal Expansion Ni Base Superalloy for Steam Turbine Applications, *Energy Mater.*, 2007, **2**(4), p 222–226.

28. A. Kumar, A. Jaiswal, M. Sanbui and S. Omar, Scandia Stabilized Zirconia-Ceria Solid Electrolyte (xSc_1CeSZ, $5 < x < 11$) for IT-SOFCs: Structure and Conductivity Studies, *Scr. Mater.*, 2016, **121**, p 10–13.

29. J. Martinsen, J.L. Stanton, R.L. Greene, J. Tanaka, B.M. Hoffman and J.A. Ibers, Metal-Spine Conductivity in a Partially Oxidized Metallomacrocycle: (Phthalocyaninato)Cobalt Iodide, *J. Am. Chem. Soc.*, 1985, **107**(24), p 6915–6920.

30. B. Shri Prakash, S. Senthil Kumar and S.T. Aruna, Properties and Development of Ni/YSZ as an Anode Material in Solid Oxide Fuel Cell: A Review, *Renew. Sustain. Energy Rev.*, 2014, **36**, p 149–179.

31. O. Yamamoto, Y. Arati, Y. Takeda, N. Imanishi, Y. Mizutani, M. Kawai and Y. Nakamura, Electrical Conductivity of Stabilized Zirconia with Ytterbia and Scandia, *Solid State Ion.*, 1995, **79**(1), p 137–142.

32. M. Xu, T. Li, M. Yang and M. Andersson, Solid Oxide Fuel Cell Interconnect Design Optimization Considering the Thermal Stresses, *Sci. Bull.*, 2016, **61**(17), p 1333–1344.

33. T.T. Molla, K. Kwok and H.L. Frandsen, Efficient Modeling of Metallic Interconnects for Thermo-Mechanical Simulation of SOFC Stacks: Homogenized Behaviors and Effect of Contact, *Int. J. Hydrog. Energy*, 2016, **41**(15), p 6433–6444.

34. T. Shimura, Z. Jiao and N. Shikazono, Dependence of Solid Oxide Fuel Cell Electrode Microstructure Parameters on Focused Ion Beam: Scanning Electron Microscopy Resolution, *Int. J. Hydrog. Energy*, 2016, **41**(47), p 22373–22380.

35. Z. Jiao and N. Shikazono, Study on the effects of polarization on local morphological change of nickel at active three-phase-boundary using patterned nickel-film electrode in solid oxide fuel cell anode, *Acta Mater.*, 2017, **135**, p 124–131.

36. F. Sun, N. Zhang, J. Li and H. Liao, Preparation of Dense Silicate Electrolyte Coating with Low Pressure Plasma Spraying and Very Low Pressure Plasma Spraying for Intermediate-Temperature Solid Oxide Fuel Cells, *J. Power Sources*, 2013, **223**, p 36–41.

37. Q.-Y. Chen, X.-Z. Peng, G.-J. Yang, C.-X. Li and C.-J. Li, Characterization of Plasma Jet in Plasma Spray-Physical Vapor Deposition of YSZ Using a < 80 kW Shrouded Torch Based on Optical Emission Spectroscopy, *J. Therm. Spray Technol.*, 2015, **24**(6), p 1038–1045.

38. S.A. Tsipas and I.O. Golosnoy, Effect of Substrate Temperature on the Microstructure and Properties of Thick Plasma-Sprayed YSZ TBCs, *J. Eur. Ceram. Soc.*, 2011, **31**(15), p 2923–2929.

39. C.-J. Li, G.-J. Yang and C.-X. Li, Development of Particle Interface Bonding in Thermal Spray Coatings: A Review, *J. Therm. Spray Technol.*, 2012, **22**(2–3), p 192–206.

40. E.-J. Yang, C.-J. Li, G.-J. Yang, C.-X. Li and M. Takahashi, Effect of Intersplat Interface Bonding on the Microstructure of Plasma-Sprayed Al_2O_3 coating, *IOP Conf. Ser. Mater. Sci. Eng.*, 2014, **61**, p 012022.

41. C.-J. Li, X.-J. Ning and C.-X. Li, Effect of Densification Processes on the Properties of Plasma-Sprayed YSZ Electrolyte Coatings for Solid Oxide Fuel Cells, *Surf. Coat. Technol.*, 2005, **190**(1), p 60–64.

42. R. Henne, Solid Oxide Fuel Cells: A Challenge for Plasma Deposition Processes, *J. Therm. Spray Technol.*, 2007, **16**(3), p 381–403.

43. P. Fauchais, A. Vardelle and B. Dussoubs, Quo Vadis Thermal Spraying?, *J. Therm. Spray Technol.*, 2001, **10**(1), p 44–66.

44. G. Antou, G. Montavon, F. Hlawka, A. Cornet and C. Coddet, Characterizations of the Pore-Crack Network Architecture of Thermal-Sprayed Coatings, *Mater. Charact.*, 2004, **53**(5), p 361–372.

45. F.L. Toma, L.M. Berger, T. Naumann and S. Langner, Microstructures of Nanostructured Ceramic Coatings Obtained by Suspension Thermal Spraying, *Surf. Coat. Technol.*, 2008, **202**(18), p 4343–4348.

46. S. Suda, M. Itagaki, E. Node, S. Takahashi, M. Kawano, H. Yoshida and T. Inagaki, Preparation of SOFC Anode Composites by Spray Pyrolysis, *J. Eur. Ceram. Soc.*, 2006, **26**(4), p 593–597.

47. C.M. An, J.-H. Song, I. Kang and N. Sammes, The Effect of Porosity Gradient in a Nickel/Yttria Stabilized Zirconia Anode for an Anode-Supported Planar Solid Oxide Fuel Cell, *J. Power Sources*, 2010, **195**(3), p 821–824.

48. S.-L. Zhang, T. Liu, C.-J. Li, S.-W. Yao, C.-X. Li, G.-J. Yang and M. Liu, Atmospheric Plasma-Sprayed $La_{0.8}Sr_{0.2}Ga_{0.8}Mg_{0.2}O_3$ Electrolyte Membranes for Intermediate-Temperature Solid Oxide Fuel Cells, *J. Mater. Chem. A*, 2015, **3**(14), p 7535–7553.

49. Z. Wang, K. Sun, S. Shen, X. Zhou, J. Qiao and N. Zhang, Effect of Co-Sintering Temperature on the Performance of SOFC with YSZ Electrolyte Thin Films Fabricated by Dip-Coating Method, *J. Solid State Electrochem.*, 2010, **14**(4), p 637–642.

50. Q. Ma, J. Ma, S. Zhou, R. Yan, J. Gao and G. Meng, A High-Performance Ammonia-Fueled SOFC Based on a YSZ Thin-Film Electrolyte, *J. Power Sources*, 2007, **164**(1), p 86–89.

51. H.Y. Jung, K.-S. Hong, H. Kim, J.-K. Park, J.-W. Son, J. Kim, H.-W. Lee and J.-H. Lee, Characterization of Thin-Film YSZ Deposited Via EB-PVD Technique in Anode-Supported SOFCs, *J. Electrochem. Soc.*, 2006, **153**(6), p A961.

52. A.V. Virkar, A Model for Solid Oxide Fuel Cell (SOFC) Stack Degradation, *J. Power Sources*, 2007, **172**(2), p 713–724.

53. A. Lussier, S. Sofie, J. Dvorak and Y.U. Idzerda, Mechanism for SOFC Anode Degradation from Hydrogen Sulfide Exposure, *Int. J. Hydrog. Energy*, 2008, **33**(14), p 3945–3951.

54. P. Tanasini, M. Cannarozzo, P. Costamagna, A. Faes, J. Van Herle, A. Hessler-Wyser and C. Comninellis, Experimental and Theoretical Investigation of Degradation Mechanisms by Particle Coarsening in SOFC Electrodes, *Fuel Cells*, 2009, **9**(5), p 740–752.

55. F.L. Lowrie and R.D. Rawlings, Room and High Temperature Failure Mechanisms in Solid Oxide Fuel Cell Electrolytes, *J. Eur. Ceram. Soc.*, 2000, **20**(6), p 751–760.

56. A. Faes, A. Nakajo, A. Hessler-Wyser, D. Dubois, A. Brisse, S. Modena and J. Van Herle, RedOx Study of Anode-Supported Solid Oxide Fuel Cell, *J. Power Sources*, 2009, **193**(1), p 55–64.

57. L. Liu, G.-Y. Kim and A. Chandra, Modeling of Thermal Stresses and Lifetime Prediction of Planar Solid Oxide Fuel Cell Under Thermal Cycling Conditions, *J. Power Sources*, 2010, **195**(8), p 2310–2318.

58. W.G. Bessler, J. Warnatz and D.G. Goodwin, The Influence of Equilibrium Potential on the Hydrogen Oxidation Kinetics of SOFC Anodes, *Solid State Ion.*, 2007, **177**(39), p 3371–3383.

59. D. Sarantaridis and A. Atkinson, Redox Cycling of Ni-Based Solid Oxide Fuel Cell Anodes: A Review, *Fuel Cells*, 2007, **7**(3), p 246–258.